Improved one-dimensional model of piezoelectric laminates for energy harvesters including three dimensional effects

Giacomo Gafforelli

Department of Civil and Environmental Engineering, Politecnico di Milano, Piazza Leonardo da Vinci 32, Milan, Italy
giacomo.gafforelli@polimi.it

Raffaele Ardito

Department of Civil and Environmental Engineering, Politecnico di Milano, Piazza Leonardo da Vinci 32, Milan, Italy raffaele.ardito@polimi.it

Alberto Corigliano

Department of Civil and Environmental Engineering, Politecnico di Milano, Piazza Leonardo da Vinci 32, Milan, Italy
alberto.corigliano@polimi.it

Abstract

The application of piezoelectric composites in energy harvesters is continuously increasing even at the microscale, with the immediate corollary of a fundamental need for improved computational tools for optimization of performances at the design level. In this paper, a refined, yet simple model is proposed with the aim of providing fast and insightful solutions to the multi-physics problem of energy harvesting via piezoelectric layered structures. The main objective is to retain a simple structural model (Euler-Bernoulli beam), with the inclusion of effects connected to the actual three-dimensional shape of the device. A thorough presentation of the analytical model is presented, along with its validation by comparison with the results of fully 3D computations.

Keywords: Piezoelectric Materials, Energy Harvesting, MEMS, Lamination Theory

1. Introduction

Piezoelectric materials have been widely used in many technological applications at the macroscopic scale. In recent times, such materials have been entering in the field of Micro-Electro-Mechanical Systems (MEMS): in particular, the coupling between electrical and mechanical behavior is feasibly used in MEMS energy harvesters (which exploit the so-called "direct effect") and actuators (based on the "indirect effect"). Piezoelectric MEMS have been proven to be an attractive technology for harvesting small magnitudes of energy from ambient vibrations. This technology promises to eliminate the need for batteries or complex wiring in microsensors/microsystems, moving closer towards battery-less, autonomous sensors systems and networks which recovered on-site the energy they need to fulfill their tasks. At the present time, most of the piezoelectric harvesters reported in the literature are cantilever laminated beams and plates with thin films

of lead zirconate titanate $Pb(Zr,Ti)O_3$ (PZT) on Si or SiNx substrate [1, 2, 3]. The multi-physics simulation of piezoelectric effects can be obtained by considering that the structural members are represented by a laminate composite with piezoelectric and silicon layers [4], the active layer is then attached to an external load resistance which reproduces the circuitry employed for the power management. Numerous models have been reported, but the effect of 3D strain field on the coupling has been considered only in few cases [5, 6]. In this paper, a simple 1D model is built in order to simulate piezoelectric thin beams and plate harvesters [7]. Starting from the fully coupled 3D constitutive equations of piezoelectricity, appropriate hypotheses are introduced to model strains and stresses so that the 1D model takes into account the 3D effects. It is worth noting that such behavior is usually neglected if the standard mechanical response of the beam is considered, in view of a small difference with respect to analytical results. Conversely, in the presence of piezoelectric coupling, the

effects connected to the actual aspect ratio of the cantilever involve a significant variation of the results in terms of electrical quantities. Consequently, the problem should be carefully studied in order to provide a reliable estimate of the energy production in a wide range of geometrical configurations. The sectional behavior of the beam is studied through the Classical Lamination Theory (*CLT*) specifically modified in order to introduce the piezoelectric coupling and a reduced order model is built through separation of time and space variables and the introduction of a suitable shape function for the beam deformation. The resulting coupled equations are solved analytically in the frequency domain and numerically in the time domain by means of step-by-step integration (α-method). For the sake of comparison, simulations have been carried out also by means of a fully 3D model implemented in a commercial code, coupled within an *ad hoc* created procedure to introduce the effect of the electrical circuit. The results show that the proposed model is in excellent agreement with the numerical outcomes, with substantial improvements with respect to the standard analytical solutions. The new constitutive equations can be employed for simulating the performances of innovative piezoelectric energy harvesters, including nonlinear [8, 9, 10], bistable and frequency-up-converter harvesters [11].

2. One dimensional model with three-dimensional effects

The piezolaminated cantilever beam is presented in figure 1, where L is the length, h the total thickness and b the width. The x_3-coordinate originates in the neutral axis and is directed downwards, x_1-coordinate lies along the beam axis while the x_2-coordinate originates in the middle of the beam, so that $-b/2 \leq x_2 \leq b/2$. A piezoelectric layer (for instance, made by PZT material) is placed on top of the beam substrate and is activated in d_{31}-mode when the beam deflects: this means that the axial deformation of the layer causes an electric field in the vertical direction (along x_3-axis).
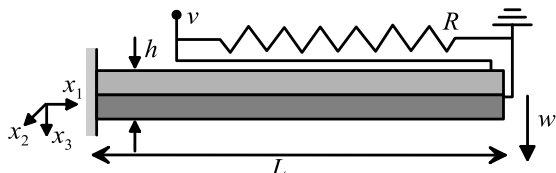

Figure 1: Cantilever piezoelectric harvester, the piezoelectric material (light grey) is placed on a structural layer (dark grey).

To implement d_{31}-mode, the polarization vector is opposite to x_3-axis and the electrodes span both the upper and the lower surfaces of PZT thin film. In this way, when the PZT layer is stretched along x_1-axis, the generated charge is collected by the electrodes. The bottom electrode is grounded while the other is attached to an external load resistance (R) which represents an ideal external circuit employed for the management of the power generated by PZT. Even though it is not developed here, the model described in the following can be easily extended to d_{33}-mode piezoelectric harvesters. The standard notation of piezoelectric analysis is adopted: stress components are denoted by the capital letter T and strain components by the capital letter S. Voigts notation is employed herein. T_{ij}, S_{ij}, E_i, D_i are stress, strain, electric field and electric displacement field components; E is the Young's modulus and v is the Poissons coefficient, e_{ij} and ε_{ii}^S are the piezoelectric stress constant and the dielectric constant computed at constant mechanical stress. It is worth noting that, in view of the geometric features of the problem, only a subset of the tensor and vector components should be explicitly involved in the analysis. The beam final stack is not homogeneous since different deposited layers are employed. The mechanical response of the layered beam can be obtained by means of a number of theories widely studied by a group at Politecnico di Torino, examined in [12]. The same group proposed a refined electro-mechanical beam formulation which uses Lagrange-type polynomials to interpolate the unknowns over the beam cross section. In such way linear, bi-linear, and quadratic approximations of the displacement and electric field over the beam cross-section are obtained [13, 14]. The electromechanical model has been used in conjunction with Carrera Unified Formulation (CUF) [15] which allows one to introduce any order expansions of the displacement unknowns over the beam section. Herein, much simpler models are used to describe the beam-cross section behavior. These assumptions limit the validity of the model to extremely thin plates and to simple shapes of the laminated structures since these hypotheses apply to microfabricated laminated structures. Herein, the cross-sections orthogonal to x_1 axis are considered to remain plane after deformation and the displacement vector results:

$$\mathbf{s} = \begin{bmatrix} -x_3 w_3' (x_1; t) \\ \hat{s}_2 (x_1, x_2, x_3, \Lambda; t) \\ y(t) + w_3 (x_1; t) + \hat{s}_3 (x_1, x_2, x_3, \Lambda; t) \end{bmatrix} \quad (1)$$

$y(t)$ denotes an external motion of the reference along x_3 axis while w_3 is the average vertical displacement of the beam cross-section ($\bullet'$ means derivative of $\bullet$ with

respect to the variable). The kinematic model presented in eq. (1) is an improvement of Euler-Bernoulli model which is justified as long as the piezoelectric beam is considered thin and the layer elastic properties are of the same order. The modification accounts for additional vertical and in-plane displacements which depend on x_2 and x_3 coordinates. In such a way, if $\hat{s}_2$ and $\hat{s}_3$ are appropriately defined, it is possible to build three dimensional stress-strain states. These displacements are also assumed to depend on a parameter which is a sort of *in-plane slenderness* of the beam defined as $\Lambda = L/b$. Functions $\hat{s}_2$ and $\hat{s}_3$ must satisfy some specific hypotheses in order to be compatible to physical stress-strain states in the beam. First, since the beam is considered thin, the in-the-thickness stress must be null, $T_{33} = 0$. Second, the in-plane stress must be $T_{22} = 0$ at $x_2 = \pm b/2$. Moreover, when $\Lambda \to 0$ the beam is infinitely wide and the strain condition $S_{22} = 0$ must always be verified; on the other hand when $\Lambda \to \infty$ the beam width is null and $T_{22} = 0$ has to be guaranteed. Considering piezoelectrics, the constitutive equations describing these two limit states read [5]:

- Null Transverse Deformation (*NTD*), $\Lambda \to 0$:
  $T_{33} = 0$ and $S_{22} = 0$

$$T_{11} = \frac{E}{1-\nu^2} S_{11} - \left(e_{31} - \frac{\nu}{1-\nu} e_{33} \right) E_3 \quad (2a)$$

$$T_{22} = \frac{E\nu}{1-\nu^2} S_{11} - \left(e_{32} - \frac{\nu}{1-\nu} e_{33} \right) E_3 \quad (2b)$$

$$S_{33} = \frac{\nu}{1-\nu^2} S_{11} - \frac{(1-2\nu)(1+\nu)}{E(1-\nu)} e_{33} E_3 \quad (2c)$$

$$D_3 = \left(e_{31} - \frac{\nu}{1-\nu} e_{33} \right) S_{11} +$$
$$+ \left(\varepsilon_{33}^S + \frac{(1-2\nu)(1+\nu)}{E(1-\nu)} e_{33}^2 \right) E_3 \quad (2d)$$

- Null Transverse Stress (*NTS*), $\Lambda \to \infty$ or $x_2 = \pm b/2$: $T_{33} = 0$ and $T_{22} = 0$

$$T_{11} = E S_{11} - (e_{31} - \nu e_{32} - \nu e_{33}) E_3 \quad (3a)$$

$$S_{22} = -\nu S_{11} + \frac{1-\nu^2}{E} \left(e_{32} - \frac{\nu}{1-\nu} e_{33} \right) E_3 \quad (3b)$$

$$S_{33} = -\nu S_{11} + \frac{1-\nu^2}{E} \left(-\frac{\nu}{1-\nu} e_{32} + e_{33} \right) E_3 \quad (3c)$$

$$D_3 = (e_{31} - e_{32}\nu - e_{33}\nu) S_{11} +$$
$$+ \left(\frac{1-\nu^2}{E} \left((e_{32} + e_{33})^2 - \frac{2e_{32}e_{33}}{1-\nu} \right) + \varepsilon_{33}^S \right) E_3 \quad (3d)$$

Moreover, in-plane electric displacement components are null accordingly to the position of electrodes.

Finally, the kinematic state given by eq. (1) must be built such that the mean shear deformations are nullified. This is guaranteed if $\hat{s}_2$ is an odd function of x_2 and neglecting all quadratic terms in x_3 (since the thickness is supposed to be small compared to other dimensions).

By imposing $T_{33} = 0$, which holds in all cases, one finds a mandatory correlation that links the in-the-thickness to the in-plane strains:

$$S_{33} = -\frac{\nu}{1-\nu} (S_{11} + S_{22}) + c_3 \quad (4)$$

where

$$c_3 = \frac{(1+\nu)(1-2\nu)}{E(1-\nu)} e_{33} E_3 \quad (5)$$

In order to recover both *NTD* and *NTS* models with a single model (Modified Transverse Deformation, MTD), eq. (3b) must be multiplied by a shape function, $f_\Lambda(x_2, \Lambda)$, that must be 1 when $\Lambda \to \infty$ or $x_2 = \pm b/2$, must be 0 when $\Lambda \to 0$ and must be even in order to assure null mean shear strain:

$$S_{22} = (-\nu S_{11} + c_2) f_\Lambda \quad (6)$$

where:

$$c_2 = \frac{1-\nu^2}{E} \left(e_{32} - \frac{\nu}{1-\nu} e_{33} \right) E_3 \quad (7)$$

The function $f_\Lambda(x_2, \Lambda)$, reported in figure 2, is given by:

$$f_\Lambda(x_2, \Lambda) = (1 - A_\Lambda(\Lambda)) |\xi|^{B_\Lambda(\Lambda)} + A_\Lambda(\Lambda) \quad (8)$$

with $\xi = 2x_2/b$ and:

$$A_\Lambda(\Lambda) = \frac{\Lambda^{a_\Lambda}}{\Lambda^{a_\Lambda} + b_\Lambda} \quad (9a)$$

$$B_\Lambda(\Lambda) = 1 + \frac{1}{\Lambda} \quad (9b)$$

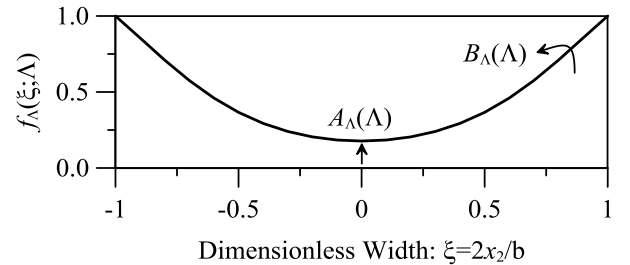where a_Λ and b_Λ are calibration parameters.

Figure 2: Shape function of in-plane strain.

Assuming eqs. (4) and (6) as strain components, the remaining stresses and electric displacement accordingly result:

$$T_{11} = \frac{E\left(1 - v^2 f_\Lambda\right)}{1 - v^2} S_{11} +$$
$$- \left(e_{31} - v f_\Lambda e_{32} - \frac{v\left(1 - v f_\Lambda\right)}{1 - v} e_{33}\right) E_3 \quad \text{(10a)}$$

$$T_{22} = (1 - f_\Lambda)\left(\frac{Ev}{1 - v^2} S_{11} +\right.$$
$$\left. - \left(e_{32} - \frac{v}{1 - v} e_{33}\right) E_3\right) \quad \text{(10b)}$$

$$D_3 = \left(e_{31} - v f_\Lambda e_{32} - \frac{v\left(1 - v f_\Lambda\right)}{1 - v} e_{33}\right) S_{11} +$$
$$+ \left(\frac{1 - v^2}{E}\left(e_{32} - \frac{v}{1 - v} e_{33}\right)^2 f_\Lambda +\right.$$
$$\left. + \frac{(1 + v)(1 - 2v)}{E(1 - v)} e_{33}^2 + \varepsilon_{33}^S\right) E_3 \quad \text{(10c)}$$

The electric potential is constant on the electrodes, grounded on the bottom electrode and free to change on the upper one (v). According to the piezoelectric constitutive law, the electric field is proportional to strain which is linear across the piezoelectric layer thickness, thus the electric potential (ϕ) should be considered quadratic across the thickness of piezoelectric. However, as long as the piezoelectric layer is thin, a linear potential can be adopted:

$$\phi = x_3^* \frac{v}{t_P} \quad \text{(11)}$$

where t_P is the piezoelectric layer thickness and x_3^* is the vertical upward coordinate in the piezoelectric layer (figure 3).
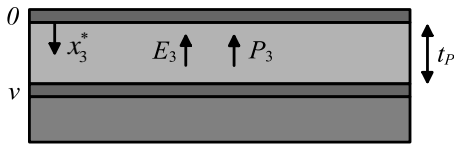

Figure 3: Polarization and electric potential between electrodes.

3. Equations of motion

The equations of motion are computed using the dissipative form of Euler-Lagrange equations:

$$\frac{\mathrm{d}}{\mathrm{d}t} \frac{\partial \mathcal{L}}{\partial \dot{q}_i} - \frac{\partial \mathcal{L}}{\partial q_i} + \frac{\partial \mathcal{D}}{\partial \dot{q}_i} = 0 \qquad \forall q_i \quad \text{(12)}$$

where $\mathcal{D}$ is the Dissipation function and $\mathcal{L}$ is the Lagrangian function which is given by:

$$\mathcal{L} = \mathcal{K} - (\mathcal{E} - \mathcal{W}) \quad \text{(13)}$$

$\mathcal{K}$, $\mathcal{E}$ are the kinetic and internal energy, respectively; $\mathcal{W}$ is the external work.

The internal energy is given by:

$$\mathcal{E} = \frac{1}{2} \int_{\mathcal{B}} (T_{11} S_{11} + T_{22} S_{22} - D_3 E_3)\, \mathrm{d}\mathcal{B} \quad \text{(14)}$$

where $\mathcal{B}$ denotes the whole volume of the laminated beam.

Given a stratification where $x_{3,k}$ is the coordinate of the k-layer and nl the total number of layers, according to eq. (10) where T_{11}, T_{22}, S_{22} and D_3 are expressed as a function of S_{11} and E_3, the internal energy results:

$$\mathcal{E} = \frac{1}{2} \int_0^L b \sum_{k=1}^{nl} \int_{x_{3,k-1}}^{x_{3,k}} \left(\hat{E}_\Lambda^k S_{11} S_{11} +\right.$$
$$\left. - \hat{e}_\Lambda^k E_3 S_{11} - \hat{\varepsilon}_\Lambda^k E_3 E_3\right) \mathrm{d}x_3 \mathrm{d}x_1 \quad \text{(15)}$$

where

$$\hat{E}_\Lambda^k = \frac{1}{b} \int_{-b/2}^{b/2} \frac{E\left(1 - v^2\right)\hat{f}_\Lambda}{1 - v^2}\, \mathrm{d}x_2 \quad \text{(16a)}$$

$$\hat{e}_\Lambda^k = \frac{1}{b} \int_{-b/2}^{b/2} \left(e_{31} - e_{32} v \hat{f}_\Lambda - \frac{v\left(1 - v \hat{f}_\Lambda\right)}{1 - v^2}\right) \mathrm{d}x_2 \quad \text{(16b)}$$

$$\hat{\varepsilon}_\Lambda^k = \frac{1}{b} \int_{-b/2}^{b/2} \left(\frac{1 - v^2}{E}\left(e_{32} - \frac{v}{1 - v} e_{33}\right)^2 \hat{f}_\Lambda +\right.$$
$$\left. + \frac{(1 + v)(1 - 2v)}{E(1 - v)} e_{33}^2 + \varepsilon_{33}^S\right) \mathrm{d}x_2 \quad \text{(16c)}$$

are averaged values of the elastic, piezoelectric and dielectric constants which also depend on the parameter Λ and:

$$\hat{f}_\Lambda(x_2, \Lambda) = f_\Lambda(x_2, \Lambda)(2 - f_\Lambda(x_2, \Lambda)) \quad \text{(17)}$$

It should be noticed that when $f_\Lambda = 1$ and $f_\Lambda = 0$ eqs. (16) reduce to the coefficients of eqs. (2) and eqs. (3). Moreover, by means of compatibility and assuming the hypotheses in eqs. (1) and (11), the strain and the electric field result:

$$S_{11} = s_1' = -x_3 w_3'' \quad \text{(18a)}$$
$$E_3 = -\phi' = -\frac{v}{t_P} \quad \text{(18b)}$$

and the internal energy writes:

$$\mathcal{E} = \frac{1}{2} \int_0^L b \sum_{k=1}^{nl} \int_{x_{3,k-1}}^{x_{3,k}} \left(\hat{E}_\Lambda^k x_3^2 w_3''^2 +\right.$$
$$\left. - 2 \frac{\hat{e}_\Lambda^k x_3}{t_P} v w_3'' - \frac{\hat{\varepsilon}_\Lambda^k}{t_P^2} v^2\right) \mathrm{d}x_3 \mathrm{d}x_1 \quad \text{(19)}$$

4

By integrating on the thickness, one obtains the generalized internal stiffness $C_{\chi\chi}$ usually defined for the theory of laminates. In such a case the new constitutive law also contains, in the integrated constitutive equations, the generalized piezoelectric coupling coefficient $C_{\chi v}$. Moreover, the same procedure is adopted on the electrical part of the constitutive law obtaining the generalized internal capacitance C_{vv} [4].

$$C_{\chi\chi} = \sum_{k=1}^{nl} \int_{x_{3,k-1}}^{x_{3,k}} \hat{E}_\Lambda^k x_3^2 \, \mathrm{d}x_3 \tag{20a}$$

$$C_{\chi v} = \sum_{k=1}^{nl} \int_{x_{3,k-1}}^{x_{3,k}} \frac{\hat{e}_\Lambda^k x_3}{t_P} \, \mathrm{d}x_3 \tag{20b}$$

$$C_{vv} = \sum_{k=1}^{nl} \int_{x_{3,k-1}}^{x_{3,k}} \frac{\hat{\varepsilon}_\Lambda^k}{t_P^2} \, \mathrm{d}x_3 \tag{20c}$$

The internal energy finally results:

$$\mathcal{E} = \frac{1}{2} \int_0^L b \sum_{k=1}^{nl} \int_{x_{3,k-1}}^{x_{3,k}} \left(C_{\chi\chi} w_3''^2 + \right.$$
$$\left. -2C_{\chi v} v w_3'' - C_{vv} v^2 \right) \mathrm{d}x_3 \mathrm{d}x_1 \tag{21}$$

The external work is given by:

$$\mathcal{W} = f_t w + \int_0^L \int_{-b/2}^{b/2} f_d w_3 \, \mathrm{d}x_2 \mathrm{d}x_1 - q v \tag{22}$$

where f_t is a tip force at the free edge, f_d is a distributed force on the top surface and q the total charge on the top electrode. The kinetic energy is given by:

$$\mathcal{K} = \frac{1}{2} \left(m_t \dot{w}^2 + J_t \dot{w}'^2 + 2M_t \dot{w}\dot{w}' + \right.$$
$$\left. + \int_0^L \int_{-b/2}^{b/2} m_d \dot{w}_3'^2 \, \mathrm{d}x_2 \mathrm{d}x_1 \right) +$$
$$+ \dot{y} \left(m_t \dot{w} + M_t \dot{w}' + \frac{1}{2} \int_0^L \int_{-b/2}^{b/2} m_d \dot{w}_3 \, \mathrm{d}x_2 \mathrm{d}x_1 \right) \tag{23}$$

where m_t, J_t and M_t are the mass and the inertial and static moment of a tip mass attached at the free edge. w and w' are the vertical displacement and the rotation of the beam evaluated at the free edge. Herein, all terms which purely depends on $\dot{y}$ have not been reported since they do not contribute when computing Euler-Lagrange equations ($\dot{\bullet}$ means derivation of $\bullet$ with respect to time); m_d is the distributed mass of the beam:

$$m_d = \sum_{k=1}^{nl} \int_{x_{3,k-1}}^{x_{3,k}} \rho^k \, \mathrm{d}x_3 \tag{24}$$

where ρ^k is the density of the k-th layer (the rotational inertia of the beam's cross-sections can be neglected as long as the beam is thin while inertial terms due to s_2 and s_3 have been neglected since they are small with respect to the longitudinal displacement).

By means of separation of variables the mechanical unknowns reduce to the displacement at the free edge:

$$w_3(x_1; t) = \psi_w(x_1) w(t) \tag{25}$$

where ψ_w is a shape function which must be chosen appropriately to boundary conditions. eq. (25) is substituted in eqs. (21)-(23) and eq. (12) is computed for both $q_1 = w$ and $q_2 = v$. Herein, A viscous dissipation function is considered:

$$\mathcal{D} = \frac{1}{2} c_M \dot{w}^2 \tag{26}$$

where c_M is the linear mechanical damping coefficient; the equation of motion is finally obtained:

$$m\ddot{w} + c_M \dot{w} + k_L 0 w - \Theta_{\chi v} v = f_{ext} - m_y \ddot{y} \tag{27a}$$
$$C_0 v + \Theta_{\chi v} w = q \tag{27b}$$

The coefficients are computed by integrating the shape function and the generalized constitutive coefficients on the area of the beam:

$$m = m_t + J_t \psi_w'^2(L) + 2M_t \psi_w'(L) +$$
$$+ \int_0^L b m_d \psi_w^2 \, \mathrm{d}x_1 \tag{28a}$$

$$m_y = m_t + M_t \psi_w'(L) + \int_0^L b m_d \psi_w \, \mathrm{d}x_1 \tag{28b}$$

$$f_{ext} = f_t + \int_0^L b f_d \psi_w \, \mathrm{d}x_1 \tag{28c}$$

$$k_L = \int_0^L b C_{\chi\chi} \psi_w''^2 \, \mathrm{d}x_1 \tag{28d}$$

$$C_0 = \int_0^L b C_v v \, \mathrm{d}x_1 \tag{28e}$$

$$\Theta_{\chi v} = \int_0^L b C_{\chi v} \psi_w'' \, \mathrm{d}x_1 \tag{28f}$$

where m is the total inertial term; m_y is the total mass activated by the external acceleration; k_L is the linear elastic stiffness; C_0 is the internal capacitance of PZT while $\Theta_{\chi v}$ is the coupling constant. The electric charge collected by the electrodes is managed by an external circuitry which provides the power supply for the self-powered electronic device. Different schemes of circuitries are investigated in [16]. The harvester provides

AC voltage and the simplest solution is the coupling with an external load resistance:

$$q = R^{-1}v \qquad (29)$$

Moreover, the power generated at the optimal load resistance is the maximum theoretical extractable power. Thus, the case studied is significant since it provides, given the harvester, the theoretical upper bound for the power generation. eq. (27) and eq. (29) are usually studied separately by commercial codes because they belong to two different physical domains which interact through electric potential and electric charge. The solution technique developed for commercial codes is explained in section 6. In case of the *MTD* code developed herein, the two physics are solved simultaneously.

$$m\ddot{w} + c_M\dot{w} + k_L w - \Theta_{\chi v} v = f_{ext} - m_y\ddot{y} \qquad (30a)$$

$$C_0\dot{v} + \Theta_{\chi v}\dot{w} + R^{-1}v = 0 \qquad (30b)$$

4. Solution in the frequency domain

The oscillator frequency response to harmonic excitations is studied through the Harmonic Balance Method [17] which provides an exact solution for linear systems. Harmonic balance mimics the spectrum analyzer in simply assuming that the response to a sinusoidal excitation ($f_{ext} - m_y\ddot{y} = F\,sin(\omega t)$) is a sinusoid at the same frequency. A couple of sinusoidal trial solutions of displacement ($w = W\,sin(\omega t)$) and voltage ($v = V\,sin(\omega t)$) is substituted in the equations, the coefficients of same harmonics are equated and the solution is computed with respect to the phasor of the response. The Frequency Response Function (FRF) results:

$$H_W = \left\{ \left[1 - \Omega_M^2 + \kappa_{\chi v}^2 \frac{\Omega_M^2}{\Omega_E^2 + \Omega_M^2} \right] + \right.$$
$$\left. + i\left[2\zeta_M\Omega_M + \kappa_{\chi v}^2 \frac{\Omega_M\Omega_E}{\Omega_E^2 + \Omega_M^2} \right] \right\}^{-1} \qquad (31)$$

whose module is the dimensionless amplitude of the displacement $Y = W/W_0$, W_0 is the static displacement, $\Omega_M = \omega/\omega_r$ is the dimensionless excitation frequency, $\omega_r = \sqrt{k_L/m}$ is the resonance angular frequency, $\Omega_E = 1/RC_0\omega_r$ is the dimensionless cut-off frequency of the circuit ($\tau_E = RC_0$ is the time constant of the RC circuit composed by the capacitance of PZT and the external load resistance) and $\kappa_{\chi v}^2 = \Theta_{\chi v}^2/k_L C_0$ is the effective piezoelectric coupling coefficient. $\kappa_{\chi v}^2$ is a global measure of the degree of coupling which takes into account both the coupling coefficient $\kappa_{31}^2 = e_{31}^2/E\varepsilon_{33}^S$ and geometrical aspects. In case

of a pure piezoelectric system, $\kappa_{\chi v}^2$ would exactly coincide with κ_{31}^2. Finally, $\zeta_M = c_M/2m\omega_r$ is the mechanical damping ratio and the quality factor is defined as $Q_M = 1/2\zeta_M$. The equivalent stiffness and the damping ratio depend on the piezoelectric coupling, on the excitation frequency and on the load resistance:

$$k_{eq} = k_L\left(1 + \kappa_{\chi v}^2 \frac{\Omega_M^2}{\Omega_E^2 + \Omega_M^2} \right) \qquad (32a)$$

$$2\zeta_{eq} = 2\zeta_M + \kappa_{\chi v}^2 \frac{\Omega_E}{\Omega_E^2 + \Omega_M^2} \qquad (32b)$$

eqs. (32) show that the presence of the piezoelectric layer affects the damping coefficient, since energy is taken out from the system, but it also increases the stiffness. The link between the displacement and the voltage is linear and is given by:

$$V = -\left(\frac{\Omega_M^2}{\Omega_E^2 + \Omega_M^2} + i\frac{\Omega_M\Omega_E}{\Omega_E^2 + \Omega_M^2} \right) \frac{\Theta_{\chi v}}{C_0} W \qquad (33)$$

The power generation is the power dissipated by the equivalent electrical damper; it results [18]

$$P = \frac{F^2\omega_r\kappa_{\chi v}^2\Omega_E\Omega_M^2}{k_L\left(\Omega_E^2 + \Omega_M^2\right)} \times$$
$$\times \left\{ \left(1 - \Omega_M^2 + \frac{\kappa_{\chi v}^2\Omega_M^2}{\Omega_E^2 + \Omega_M^2} \right)^2 + \left(2\zeta_M\Omega_M + \frac{\kappa_{\chi v}^2\Omega_M\Omega_E}{\Omega_E^2 + \Omega_M^2} \right)^2 \right\}^{-1} \qquad (34)$$

The power can be maximized with respect to the electric load, or similarly to the cut-off frequency:

$$\Omega_E^{opt} = \Omega_M\sqrt{\frac{\left(1 - \Omega_M^2 + \kappa_{\chi v}^2\right)^2 + 4\zeta_M^2\Omega_M^2}{\left(1 - \Omega_M^2\right)^2 + 4\zeta_M^2\Omega_M^2}} \qquad (35)$$

eq. (35) shows that for maximizing the power, the external load resistance should be calibrated accordingly to the frequency of the solicitation.

5. Solution in the time domain

Hughes α-method [19] has been chosen to solve eq. (30) for time dependent solicitations. The equations are rearranged in matrix formulation in the variable $\mathbf{x}^\top = [w \quad v]$:

$$\mathbf{M}\ddot{\mathbf{x}} + \mathbf{C}\dot{\mathbf{x}} + \mathbf{K}\mathbf{x} = \mathbf{F} \qquad (36)$$

where:

$$\mathbf{M} = \begin{bmatrix} m & 0 \\ 0 & 0 \end{bmatrix} \tag{37a}$$

$$\mathbf{C} = \begin{bmatrix} c_M & 0 \\ \Theta_{\chi v} & C_0 \end{bmatrix} \tag{37b}$$

$$\mathbf{K} = \begin{bmatrix} k_L & -\Theta_{\chi v} \\ 0 & R^{-1} \end{bmatrix} \tag{37c}$$

$$\mathbf{F} = \begin{bmatrix} f_{ext} - m_y \ddot{y} \\ 0 \end{bmatrix} \tag{37d}$$

The method has been implemented and solved in a MATLAB code.

6. 3D Finite Element model

In order to validate the model explained in sections 2-5 a commercial code, ABAQUS, is employed. The code allows using piezoelectric constitutive equations in the classical structural mechanic environment. However, only 3D models can be built, this is an enormous limitation since piezoelectric elements are usually employed in laminated beams or plates. This results in a large numerical effort since a high number of elements must be employed to correctly reproduce the behavior of high aspect ratio components. Moreover, the solver of lumped electrical circuitry is not available in ABAQUS. For what concerns the solution of piezoelectric behavior, the code solves an equation similar to eq. (27) built on the basis of 3D finite elements augmented with the additional voltage degree of freedom. The voltage is grounded on the bottom surface of piezoelectric material while is constrained to be uniform on the top surface, this to reproduce the presence of electrodes. The electric charge plays the role played in structural mechanics by the external force. The connection with the electric circuit has been built *ad hoc* through an external subroutine which interacts in a staggered procedure through the electric potential and the electric charge which act respectively as variable and load in the piezoelectric module and as load and variable in the electric module. The scheme of the solving algorithm including the subroutine is shown in figure 4. In this study the subroutine reduces to a discrete version of Ohm's law, but there is not any particular limitation on the equations that could be implemented.
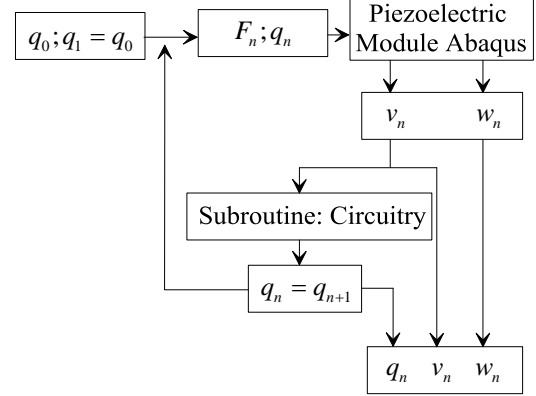
Figure 4: Algorithm for the resolution of the coupled piezoelectric-electric problem.

The explicit algorithm can be considered correct as long as the variation of the charge in every step is small and the difference in the voltage computed with q_n and q_{n+1} is negligible. This is obtained for a small enough time step (Δt). In case of a pure resistive circuit, the stability of the algorithm is assured only if the time step is lower than the time constant of the RC circuit ($\Delta t < RC_0$). Comparative analyses have been performed to validate the model. A 2 layers (2 μm PZT on 6 μm silicon substrate) cantilever beam has been chosen. The length is 1000 μm, the width is parametric and varies from 50 μm to 5000 μm. Geometrical and material properties of the layers are given in table 1.

Table 1: Material parameters values of the cantilever MEMS harvester, $\varepsilon_0 = 8.854 \ 10^{-12}$ F/m.

	ρ [g/cm^3]	E [GPa]	ν [-]
PZT	7.70	100	0.30
PolySilicon	2.33	148	0.33

	e_{31} [N/mV]	e_{33} [N/mV]	ε_{33}^S [ε_0]
PZT	-12	20	2000
PolySilicon	0	0	0

Convergence analyses (figure 5 and figure 6) show that a good approximation can be rapidly obtained employing quadratic elements. The chosen mesh is reported in figure 5 and counts 40 quadratic elements on the length and an element for each layer on the thickness (as shown by figure 7).
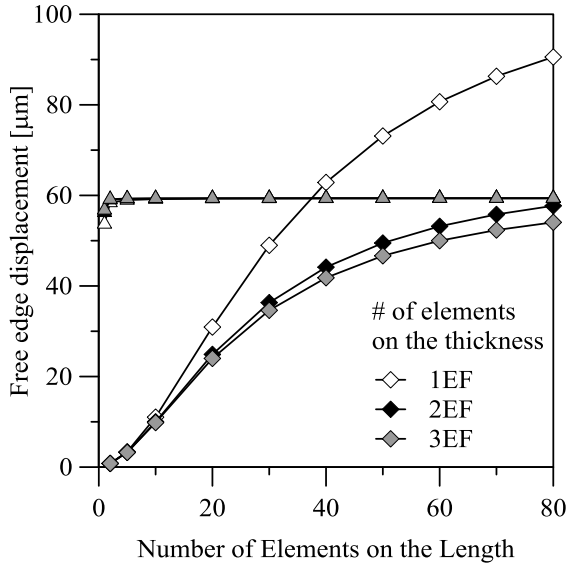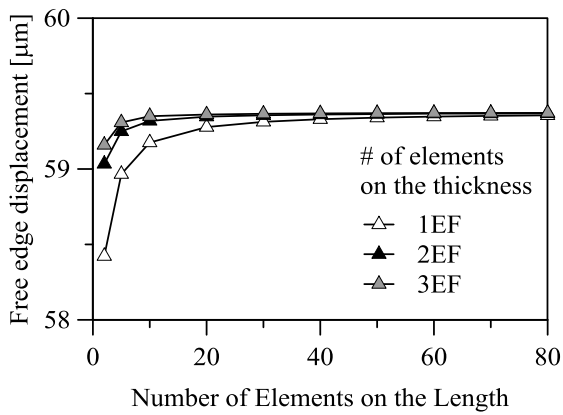
Figure 5: Convergence analysis, linear finite elements.

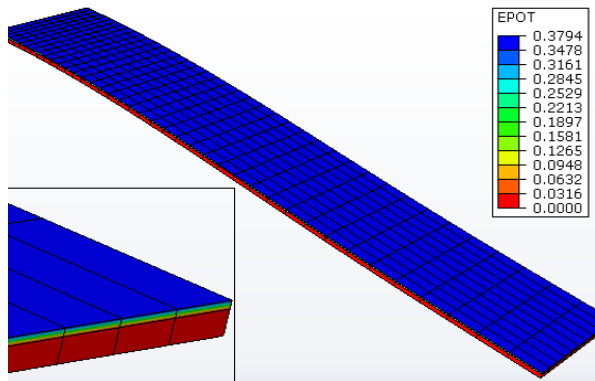Figure 6: Convergence analysis, quadratic finite elements.

Figure 7: 3D Mesh in ABAQUS.

7. Static analyses

Open circuit static analyses have been performed with a tip load $F = 1$ μN/μm at the beam free edge and null external acceleration. The classical models have been compared to the modified model which has been calibrated with respect to ABAQUS analyses. The resulting calibrated parameters are $a_\Lambda = 0.8$ and $b_\Lambda = 2.2$. The response of classical models is constant with respect to the width while the response of the modified model correctly describes the variation in stiffness (figure 8) and more important, the variation of the upper electrode voltage and correspondingly of coupling coefficient (figure 9). From the mechanical point of view the mean error can be reduced from 8% to less than 1%, while the error on the voltage reduces from 27% to less than 3%. Considering that the power will be proportional to the voltage squared, the reduction of the error in the power generation is expected to be even more significant.
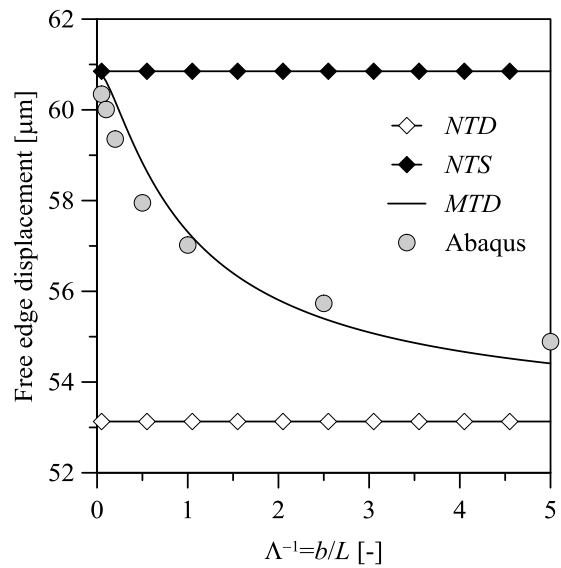
Figure 8: Open circuit Static Analysis, Displacement.

8
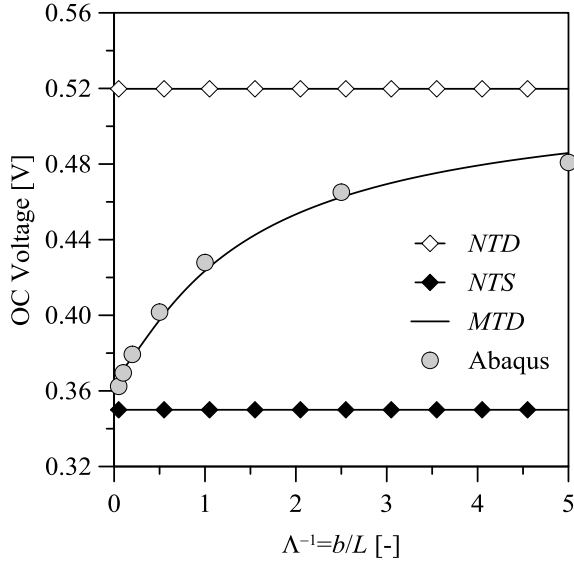
Figure 9: Open circuit Static Analysis, Voltage.

8. Frequency analyses
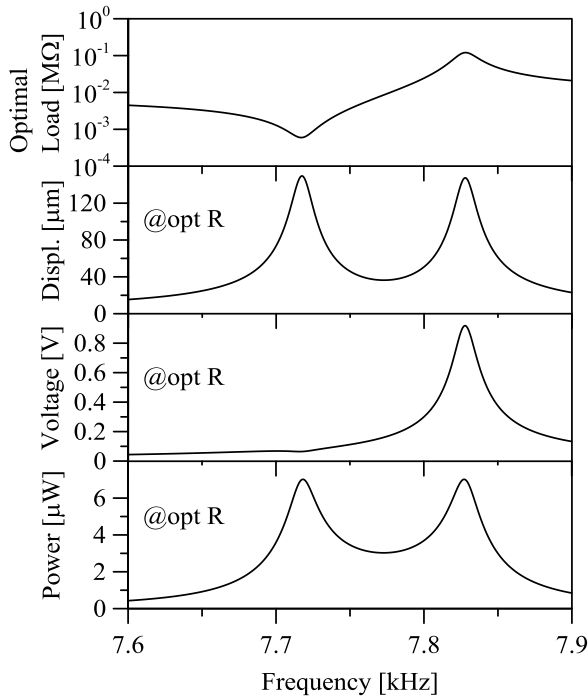
Figure 10: Frequency response, max $\ddot{y}$ = 90 g, b = 200 μm, Q_M = 500, optimal R.

The analytical solution of the frequency response has been computed for the aforementioned device considering null external forces and an external acceleration

of 90 g. The frequency response (figure 10) computed at the optimal load resistance shows two peaks that occur near the mechanical resonance frequency and near a second frequency called anti-resonance.

The peaks would perfectly occur at these frequencies if mechanical damping had been neglected. The presence of two peaks is physically explained by the fact that the power ($P = v^2/R$) can be maximized both at high resistance (high voltage) and at low voltage (low resistance). It can be shown that in a general case the peaks are obtained when the injected electrical damping equals the mechanical damping of the system [20].

Figure 11 shows that classical models cannot describe the dependence of resonance frequencies ($f_r = \omega_r/2\pi$) on the width of the device. On the other hand, the modified model qualitatively reproduces the variation in frequency. It still does not perfectly match with 3D numerical results because of a mismatch in the computation of the modal mass associated to the first vibrating mode. This error could be probably be fixed by enriching the beam cross sectional behavior as proposed in CUF [21] which proposed the computation and the evaluation of higher-order theories for free vibration analysis of beams.

Conversely to the resonance frequency, which is a pure mechanical parameter, the anti-resonance frequency (f_{ar}) depends on the effective piezoelectric coupling coefficient and it measures the global coupling:

$$f_{ar} = f_r \sqrt{1 + \kappa_{\chi v}^2} \qquad (38)$$
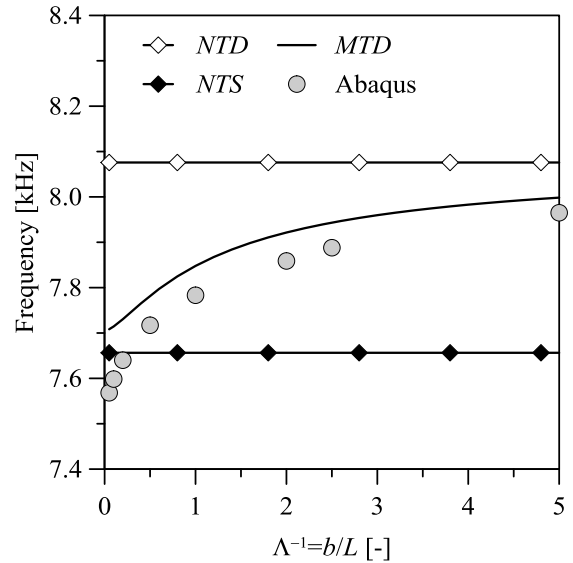
Figure 11: Resonance frequency.
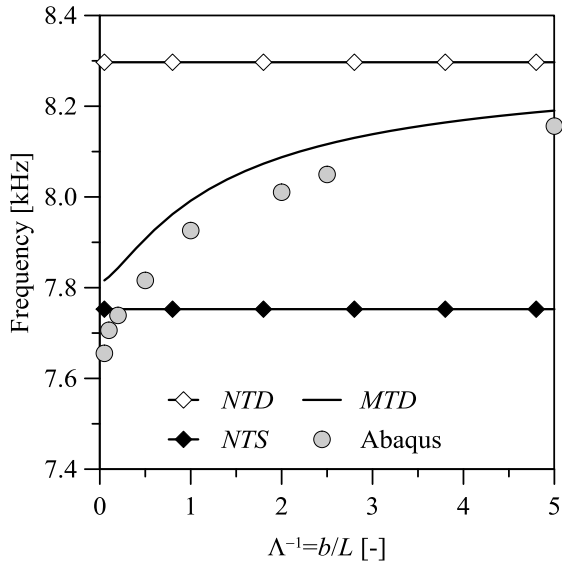
Figure 12: Anti-Resonance frequency.

Figure 14: Voltage, $b = 200$ μm, $Q_M = 500$.

Figure 12 shows that a good agreement is also obtained for the anti-resonance frequency. This result is profoundly different from the previous since anti-resonance depend on the electrical parameters while the resonance depends on mechanical ones. This means that the model can correctly describe the variation of elastic modulus, coupling coefficient and dielectric constant depending on different width ratio. To better understand the frequency response computed in section 4, three-dimensional plots of displacement, voltage and power generation are represented in figures 13-15. The classical two peaks power generation response is obtained.
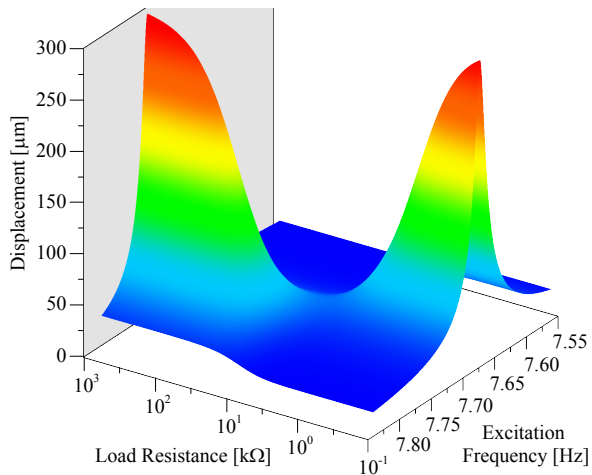
Figure 13: Displacement, $b = 200$ μm, $Q_M = 500$.
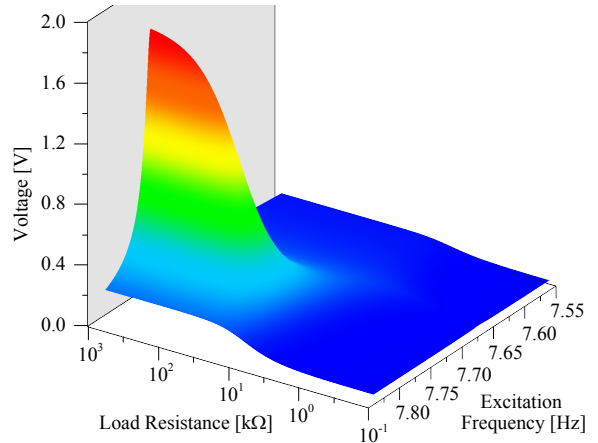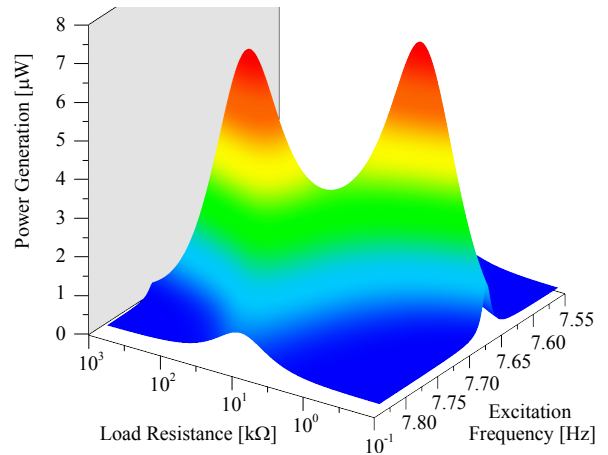
Figure 15: Power generation, $b = 200$ μm, $Q_M = 500$.

10

9. Quasi-Static analyses
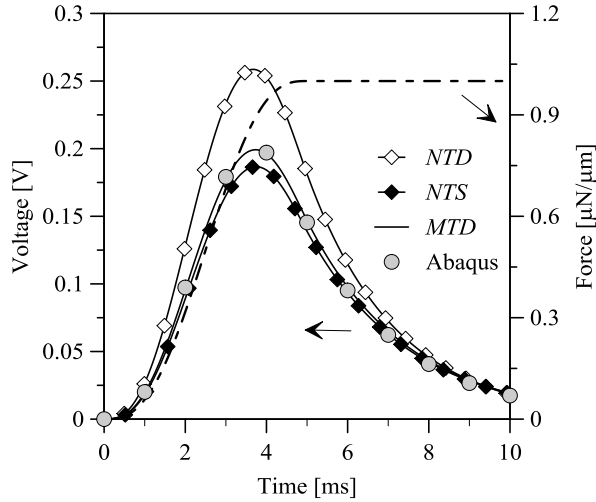
Figure 16: Quasi Static analysis, b = 200 μm, R = 1 MΩ, Voltage and Force.

Figure 17: Quasi Static analysis, b = 200 μm, Voltage.

Quasi static analyses have been performed; a smooth step load followed by a constant plateau has been considered. The dashed line in figure 16 reproduces the applied force (right axis) vs. time. The maximum reached force is F = 1 μN/μm. The load resistance is varied as parameter and it is shown that the voltage gradually decreases to zero because the external load resistance dissipates energy reducing the charge on the electrodes. The decreasing speed depends on the value of the resistance, the lower the resistance, the faster the voltage decreases while in open circuit the resulting voltage remains constant since no energy is harvested. Parametric analyses have been performed varying the load resistance with b = 200 μm (figure 17-18) and b = 2000 μm (figure 19-20) . It is clear that when $R \rightarrow \infty$ the solution should collapse to the open circuit solution of figure 9. While when $R \rightarrow 0$ short circuit condition is obtained and no power can be harvested. In this case, the influence of the electrical domain is nullified and the oscillator reduces to a pure mechanical one. A peak power generation is obtained for an optimal value of load resistance which inversely depends on the capacitance of the device. All models predict the same optimal load resistance as ABAQUS.

As expected, the voltage range does not significantly change from the 200 μm to the 2000 μm device since both the coupling constant and the capacitance depend linearly on the width and the voltage is proportional to their ratio. On the other hand, the power generation increases (barely linearly) while increasing the width because of the influence of the external resistance. Indeed, the optimal resistance inversely depends on the width of the device.

This same analysis has been performed for different values of width and the peak power per unit width, computed at the optimal load resistance, has been collected in figure 21 for all models. It is shown that the *MTD* model correctly predicts a cantilever type harvester for all range of length-beam ratios that have been considered. On the other hand *NTD* and *NTS* models predict that the power generation is linear to the width and they always under- and overestimate voltage and power, respectively. As shown by figure 22 the mean error on the power generation can be reduced from about 30% to less than 5% considering both models. It can also be concluded that wider harvesters not only recover more power, which is obvious, but also have a higher power density than narrower beams.
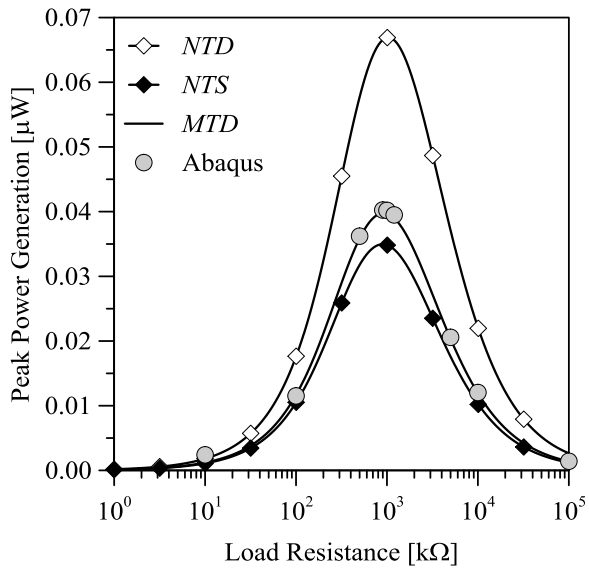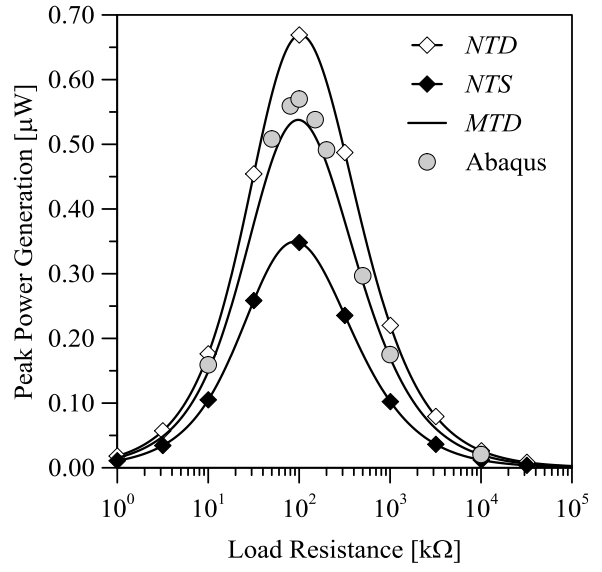
11

Figure 18: Quasi Static analysis, $b = 200$ μm, Power.
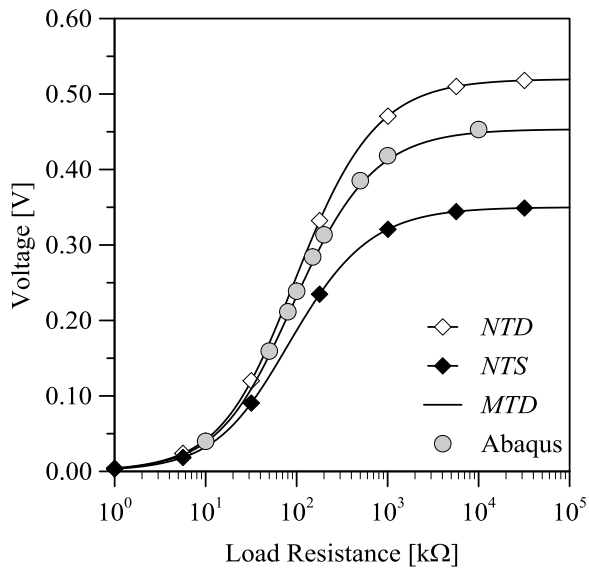

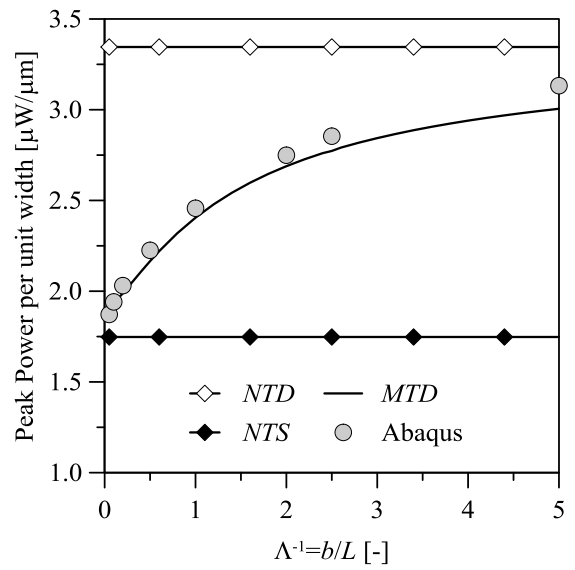Figure 20: Quasi Static analysis, $b = 200$ μm, Power.

Figure 21: Peak Power generation at Optimal R.

10. Dynamic analyses

Free oscillation analyses have been performed on the same structure introduced in section 7. As before, the beam is quasi-statically moved to a certain position but now is suddenly released and left free to oscillate. The width is fixed to $b = 200$ μm while the load resistance and the mechanical quality factor are tuned as parameters.

Figure 19: Quasi Static analysis, $b = 2000$ μm, Voltage.

12
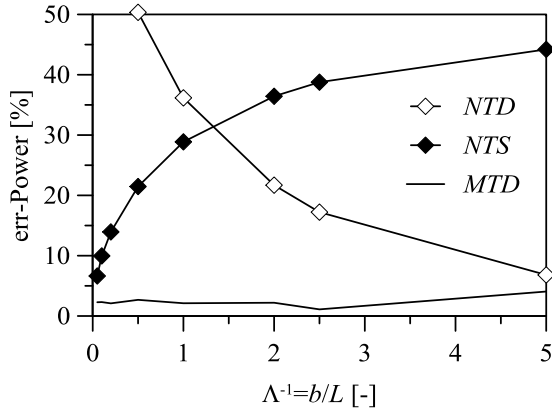
Figure 22: Error on Power Generation.

The mechanical damping has been introduced in ABAQUS through Rayleigh method:

$$\mathbf{C} = \alpha_R \mathbf{M} + \beta_R \mathbf{K} \qquad (39)$$

by setting:

$$\alpha_R = \omega_r Q_M \qquad (40a)$$
$$\beta_R = 0 \qquad (40b)$$
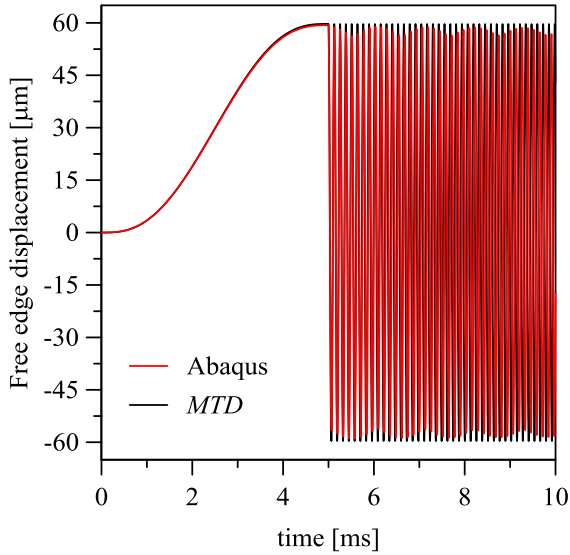
Figure 23: Displacement, $b = 200$ μm, $R = \infty$, $Q_M = \infty$.

Figure 23 and figure 24 show the free oscillations of an harvester in case of null mechanical damping at infinite and optimal R. It is clear that the presence of the electrical load correctly damps the oscillation converting mechanical energy into electrical power. It has to be

noted, that the damping in figure 24 comes only from the coupling with the electronics.
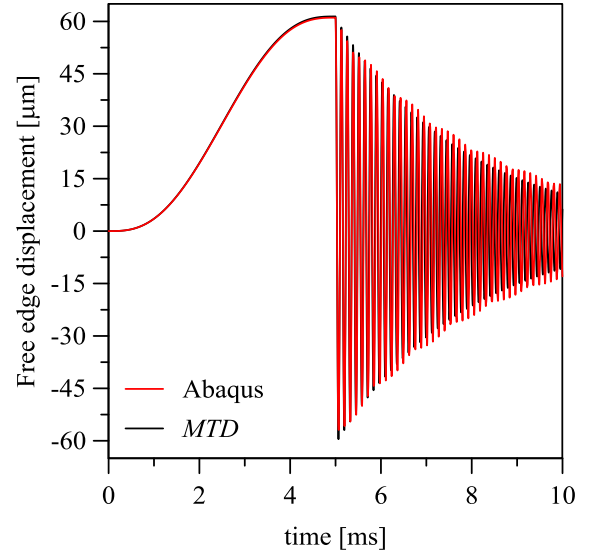
Figure 24: Displacement, $b = 200$ μm, optimal R, $Q_M = \infty$.
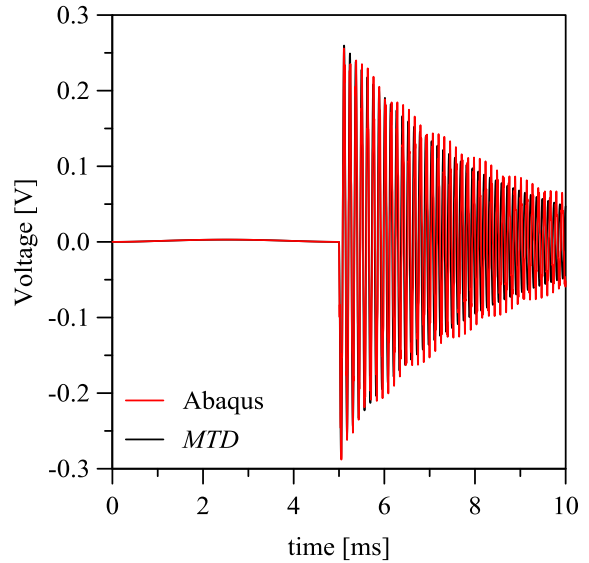
Figure 25: Voltage, $b = 200$ μm, optimal R, $Q_M = \infty$.

The first significant result is that while the *MTD* code took less than 3 seconds to perform the analysis, ABAQUS required 5 hours 25 minutes and 23 seconds to produce such results. This is easily explained by the fact that ABAQUS implemented a 3D fully coupled model solved in implicit dynamics. One may object that the *MTD* model can only be employed in simple cases.

However, the validity of the model lasts as long as the piezoelectric material is employed in thin film deposited on a substrate and this is the case of a large number of applications, particularly in MEMS. Figure 25 and figure 26 report the voltage and power generated by the harvester at optimal load resistance.
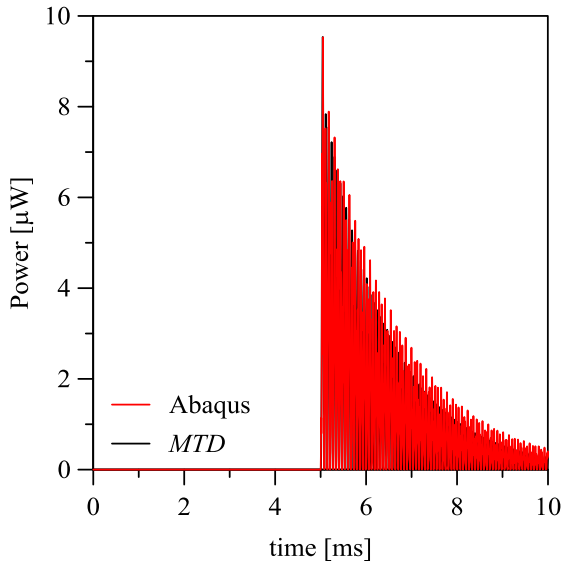

Figure 26: Power, $b = 200$ μm, optimal R, $Q_M = \infty$.

the beam. Higher order frequencies introduce a lower wavelength perturbation superimposed to the first mode oscillation. Thus, they mainly affect the voltage. Moreover, the influence of higher modes becomes predominant at lower external load resistances (figure 29).
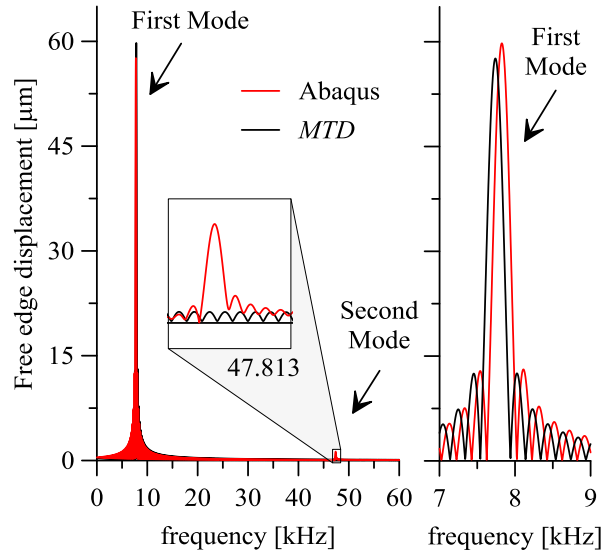

Figure 27: Fourier's transform of the free oscillations of the harvester $b = 200$ μm, $Q_M = \infty$, $R \rightarrow \infty$.
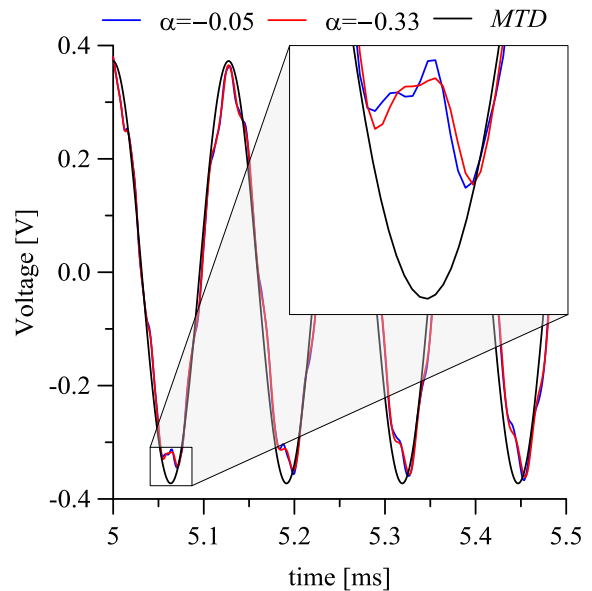
Two things have to be noticed from previous results. First, ABAQUS and MATLAB solutions are perfectly matched in the initial phase of the oscillation while they slightly shift in the ending part. This is due to the small mismatch in resonance frequencies which was already revealed in figure 11 and figure 12 and is newly highlighted in figure 27 which shows the Fourier's transform of the results. Second, ABAQUS solution shows a second frequency which produces a small oscillation of the peak values of the responses. This effect is not due to numerical errors since is not eliminated by tuning the numerical damping coefficient α of Hughes integration scheme but rather it originates from higher order resonance frequencies which are completely neglected in the *MTD* model since only a single shape function has been employed. On the contrary, in ABAQUS, the sudden jump activates all modal frequencies. This phenomenon is much more visible in the voltage plot (figure 28). This happens because the displacement variable is measured at the free edge and it is less sensitive to the perturbations that occur in the remaining portion of the beam. On the contrary the voltage is constrained to be constant all over the upper and bottom surfaces of PZT, hence it is a sort of mean value computed on the whole length of

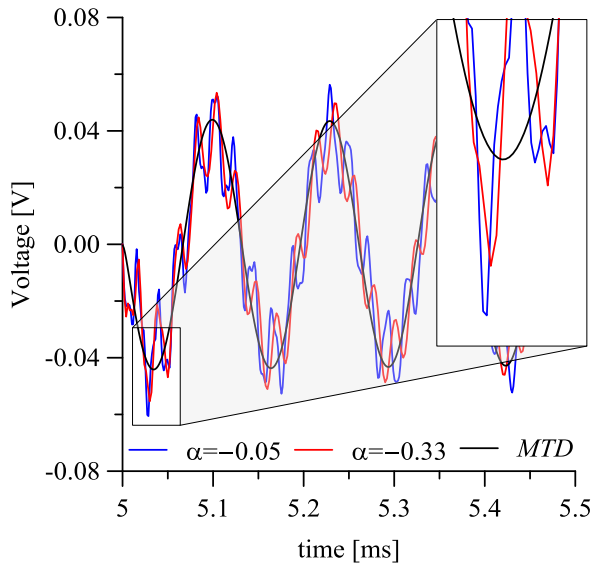Figure 28: Influence of high order frequencies on the voltage, $b = 200$ μm, $Q_M = \infty$, $R \rightarrow \infty$.

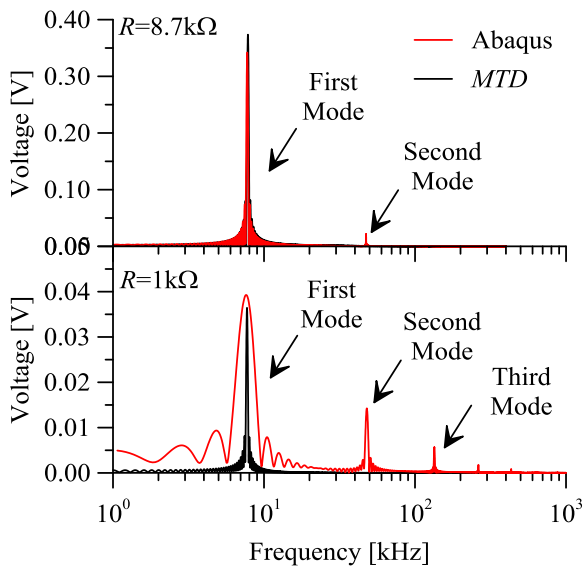Figure 29: Influence of high order frequencies on the voltage, $b = 200$ μm, $Q_M = \infty$, $R = 1$ kΩ.

Figure 30: Fourier's transform of the free oscillations of the harvester, $b = 200$ μm, $Q_M = \infty$, $R = 1$ kΩ.

Low R means low time constant of the RC circuit composed by the internal capacitance of PZT and the external load resistance. Thus, the charge in the PZT capacitor can be moved faster resulting in more sensitivity to higher frequencies. Figure 30 shows how the Fourier's transform of the resulting voltage changes at different load resistances. Accordingly to these results it is expected that the *MTD* model underestimates the

peak voltage (so the peak power generation) at low resistances. The results of parametric analyses at varying R have been collected in figure 31. As expected the *MTD* model better reproduces numerical results than plane and uniaxial stress models.
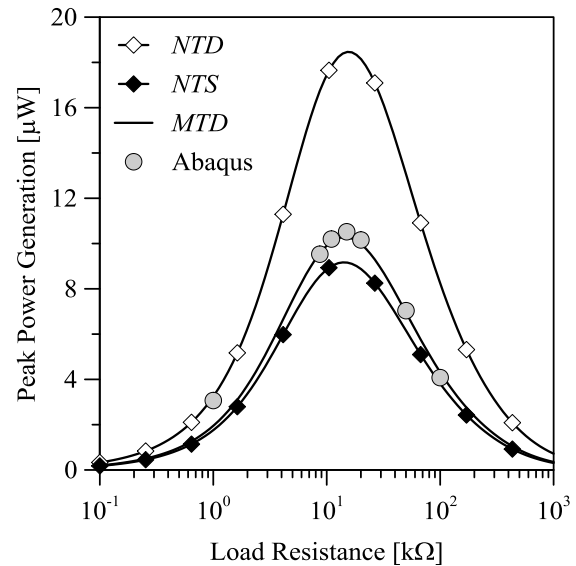

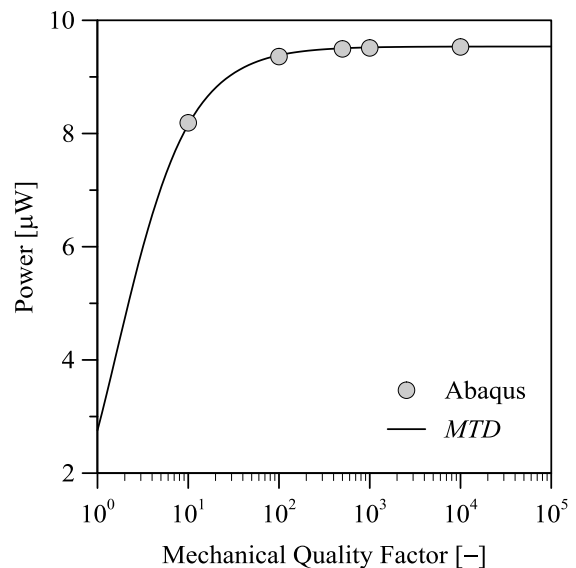Figure 31: Dynamic analysis, Peak power generation, $b = 200$ μm, $Q_M = \infty$.

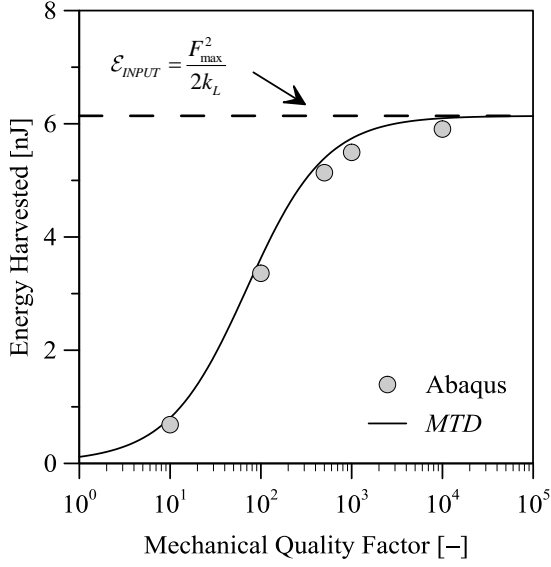Figure 32: Influence of Q_M on peak power generation, $b = 200$ μm, $R = 8.7$ kΩ.

15

Figure 33: Influence of Q_M on total energy harvested, $b = 200$ μm, $R = 8.7$ kΩ.
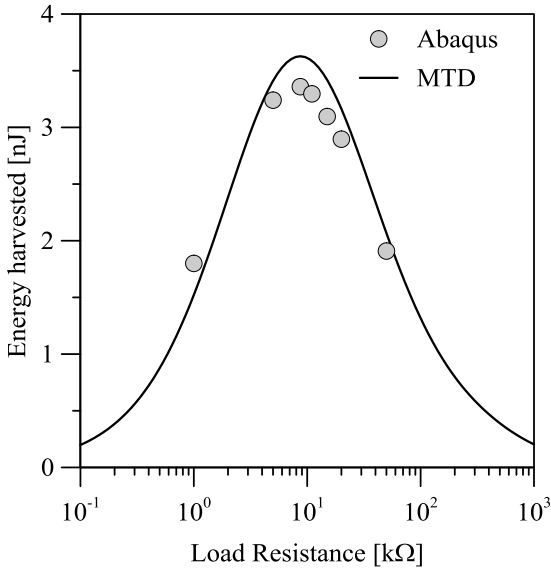

Figure 34: Influence of R on total energy harvested, $b = 200$ μm, $R = 8.7$ kΩ.

The influence of the mechanical quality factor on the peak power generation is reported in figure 32. Except for significant low values of Q_M, the peak power generation remains more or less constant. This does not mean that the mechanical damping has no influence on the performances of the harvester. In fact, figure 33 shows that the total energy harvested reduces as Q_M decreases. When no mechanical damping is considered, the whole

energy injected into the system is harvested:

$$\mathcal{E}_{OUTPUT} = \mathcal{E}_{INPUT} = \frac{F_{max}^2}{2k_L} \qquad (41)$$

As the peak power generation changes with the load resistance also the energy harvested is modified by the choice of the load (figure 34).
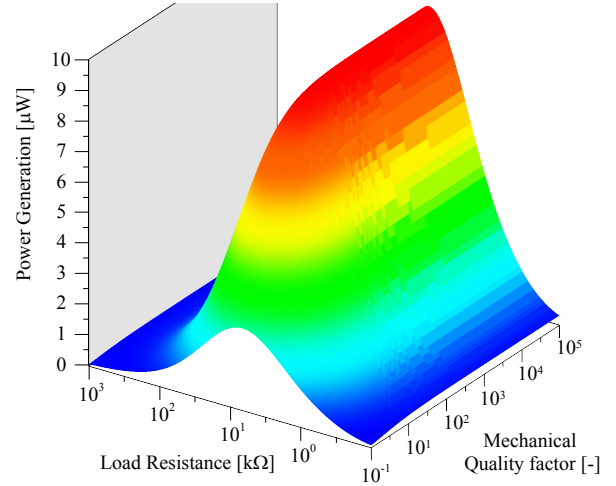

Figure 35: Influence of R and Q_M on peak power generation, $b = 200$ μm.

The peak power generation and the energy harvested are collected in figure 35 and figure 36 where it is shown that both the power and the energy increase as the quality factor increases.
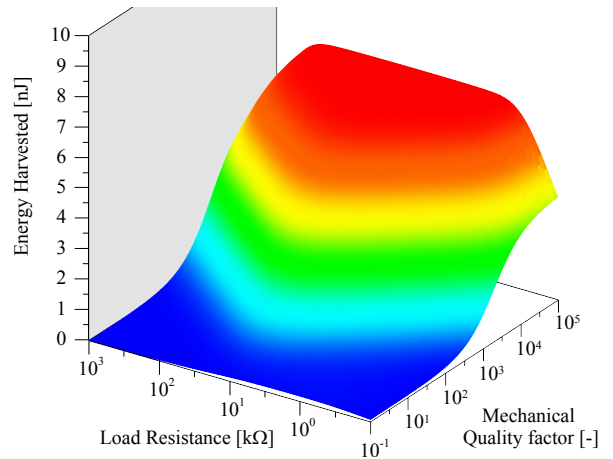

Figure 36: Influence of R and Q_M on total energy harvested, $b = 200$ μm.

It has to be noted that the peak power generation and the peak energy harvested do not occur at the

16

same load resistance. The peak power is reached at $R = 15$ kΩ while the peak energy harvested is obtained at $R = 1/C_0\omega_r = 8.7$ kΩ. This value designs the optimal load resistance associated to the harvester.

11. Conclusion

A simple 1D model (Modified Transverse Deformation Model, *MTD*) has been built to perform multi-physics simulation for MEMS piezoelectric harvesters. Suitable hypotheses on stresses and strains have been implemented to take into account 3D effects on elastic and electric parameters. A mixed theory which includes the effect of the transverse strain has been considered such that boundary conditions and limit stress and strain configurations are recovered. The piezolaminated beam with modified elastic and electric constants has been studied through the Classical Lamination Theory (*CLT*) specifically modified to introduce the piezoelectric coupling and a lumped parameters model has been built through separation of variables. An extension to Finite Element method can be easily introduced. The resulting coupled equations have been analytically solved in the frequency domain and have been numerically solved in the time domain by means of α-method. The aforementioned model has been validated by comparison with fully 3D multi-physics simulations performed by a commercial code (ABAQUS) where an external subroutine has been added to simulate the coupling with an external load resistance. The comparison with the commercial codes shows that the *MTD* model is accurate enough to reproduce qualitatively and quantitatively the response of the harvester gaining in terms of model dimensions and computational time, in particular when performing step-by-step time analysis. The validated model can be used to perform simulations on MEMS scale piezoelectric energy harvesters. Moreover, the developed constitutive law can be applied to thin piezolaminated beam energy harvesters that exploit advanced designs for maximizing the conversion of energy: e.g. nonlinearity [22], including bistability [23] and frequency-up-conversion [11].

Acknowledgment

References

[1] S. Roundy, P. K. Wright, A piezoelectric vibration based generator for wireless electronics, Smart Materials and Structures 13 (5) (2004) 1131–1142. doi:10.1088/0964-1726/13/5/018.

[2] Y. B. Jeon, R. Sood, J.-H. Jeong, S.-G. Kim, MEMS power generator with transverse mode thin film PZT, Sensors and Actuators A: Physical 122 (1) (2005) 16–22. doi:10.1016/j.sna.2004.12.032.

[3] S.-G. Kim, S. Priya, I. Kanno, Piezoelectric MEMS for energy harvesting, MRS Bulletin 37 (11) (2012) 1039–1050. doi:10.1557/mrs.2012.275.

[4] R. Ardito, E. Bertarelli, A. Corigliano, G. Gafforelli, On the application of piezolaminated composites to diaphragm micropumps, Composite Structures 99 (2013) 231–240. doi:10.1016/j.compstruct.2012.11.041.

[5] C. Maurini, J. Pouget, F. Dell'Isola, On a model of layered piezoelectric beams including transverse stress effect, International Journal of Solids and Structures 41 (16-17) (2004) 4473–4502. doi:10.1016/j.ijsolstr.2004.03.002.

[6] C. Maurini, J. Pouget, F. Dell'Isola, Extension of the Euler-Bernoulli model of piezoelectric laminates to include 3D effects via a mixed approach, Computers \& Structures 84 (22-23) (2006) 1438–1458. doi:10.1016/j.compstruc.2006.01.016.

[7] G. Gafforelli, R. Ardito, A. Corigliano, C. Valzasina, F. Procopio, Numerical simulations of piezoelectric MEMS energy harvesters, in: 15th International Conference on Thermal, Mechanical and Multi-Physics Simulation and Experiments in Microelectronics and Microsystems, EuroSimE 2014, 2014.

[8] B. P. Mann, D. A. Barton, B. A. Owens, Uncertainty in performance for linear and nonlinear energy harvesting strategies, Journal of Intelligent Material Systems and Structures 23 (13) (2012) 1451–1460. doi:10.1177/1045389X12439639.

[9] A. Erturk, D. Inman, Broadband piezoelectric power generation on high-energy orbits of the bistable Duffing oscillator with electromechanical coupling, Journal of Sound and Vibration 330 (10) (2011) 2339–2353. doi:10.1016/j.jsv.2010.11.018.

[10] G. Gafforelli, A. Corigliano, R. Xu, S.-g. Kim, Experimental verification of a bridge-shaped , nonlinear vibration energy harvester, Applied Physics Letters 203901 (105). doi:10.1063/1.4902116.

[11] R. L. Harne, K. W. Wang, A review of the recent research on vibration energy harvesting via bistable systems, Smart Materials and Structures 22 (2) (2013) 023001. doi:10.1088/0964-1726/22/2/023001.

[12] D. Ballhause, M. D'Ottavio, B. Kröplin, E. Carrera, A unified formulation to assess multilayered theories for piezoelectric plates, Computers \& Structures 83 (15-16) (2005) 1217–1235. doi:10.1016/j.compstruc.2004.09.015.

[13] F. Miglioretti, E. Carrera, M. Petrolo, Variable kinematic beam elements for electro-mechanical analysis, Smart Structures and Systems 13 (2014) 517–546. doi:10.12989/sss.2014.13.4.517.

[14] F. Miglioretti, E. Carrera, Application of a Refined Multi-Field Beam Model for the Analysis of Complex Configurations, Mechanics of Advanced Materials and Structures 22 (September 2014) (2014) 52–66. doi:10.1080/15376494.2014.912365.

[15] E. Carrera, A. Ciuffreda, A unified formulation to assess theories of multilayered plates for various bending problems, Composite Structures 69 (3) (2005) 271–293. doi:10.1016/j.compstruct.2004.07.003.

[16] D. Guyomar, A. Badel, E. Lefeuvre, C. Richard, Toward energy harvesting using active materials and conversion improvement by nonlinear processing, IEEE Transactions on Ultrasonics, Ferroelectrics and Frequency Control 52 (4) (2005) 584–595. doi:10.1109/TUFFC.2005.1428041.

[17] K. Worden, G. R. Tomlinson, Nonlinearity in Structural Dynamics, i Edition, IOP Publishing Ltd, London, 2001. doi:10.1887/0750303565.

[18] N. E. Du Toit, B. L. Wardle, S.-G. Kim, Design Considerations for Mems-Scale Piezoelectric Mechanical Vibration Energy Harvesters, Integrated Ferroelectrics 71 (1) (2005) 121–160. doi:10.1080/10584580590964574.

[19] T. J. R. Hughes, The Finite Element Method, i Edition, Prentice-Hall, Englewood Cliffs, 1987.

[20] J. M. Renno, M. F. Daqaq, D. J. Inman, On the optimal energy harvesting from a vibration source, Journal of Sound and Vibration 320 (1-2) (2009) 386–405. doi:10.1016/j.jsv.2008.07.029.

[21] E. Carrera, F. Miglioretti, M. Petrolo, Computations and evaluations of higher-order theories for free vibration analysis of beams, Journal of Sound and Vibration 331 (19) (2012) 4269–4284. doi:10.1016/j.jsv.2012.04.017.

[22] G. Gafforelli, R. Xu, A. Corigliano, S.-G. Kim, Modeling of a Bridge-Shaped Nonlinear Piezoelectric Energy Harvester, Energy Harvesting and Systems (ISSN (Print) 2329-8774) (2014) ISSN (Online) 2329–8766. doi:10.1515/ehs-2014-0005.

[23] M. F. Daqaq, R. Masana, A. Erturk, D. Dane Quinn, On the Role of Nonlinearities in Vibratory Energy Harvesting: A Critical Review and Discussion, Applied Mechanics Reviews 66 (4) (2014) 040801. doi:10.1115/1.4026278.